Apollo 14 Mare Basalt Petrogenesis: Assimilation of KREEP-Like Components by a Fractionating Magma

Clive R. Neal and Lawrence A. Taylor

Department of Geological Sciences, University of Tennessee, Knoxville, TN 37996

Marilyn M. Lindstrom*

Department of Earth and Planetary Sciences, Washington University, St. Louis, MO 63130

Now at NASA Johnson Space Center, Code SN2, Houston, TX 77058

Whole rock and mineral data from 22 new 14321 high-Al (HA) mare basalts demonstrate a complicated petrogenesis for these rocks. The trace element characteristics of these basalts exhibit considerable variation that cannot be related to short-range unmixing alone. This variation is facilitated by the combined effects of KREEP assimilation and fractional crystallization of liquidus phases (AFC). Such a process is reflected in the REE profiles, which range from flat, primitive types to LREE-enriched (KREEP-like), evolved types. Earlier work on Apollo 14 HA mare basalts had defined five groups. We suggest this is an artifact of sampling; when the new data are added, a continuum of compositions is observed. Detailed trace element modeling demonstrates that a primitive parental magma (taken as 14321,1422: La = 3.19 ppm; La/Lu = 7.2; SiO_2 = 46%; MgO = 11%) evolves by AFC with KREEP. The ratio of mass assimilated to mass crystallized ("r" value) is 0.22. Proportions of crystallizing phases vary as fractional crystallization proceeds. Major element modeling indicates that only olivine (90%) and chromite (10%) are precipitated during the first 14% of crystallization. Plagioclase, olivine, and chromite (50:40:10) fractionate as crystallization proceeds, and finally opx, plagioclase, and ilmenite (60:30:10) fractionate together after 21% crystallization. It is envisaged that this AFC process occurs at depth within the lunar crust and the fractionating phases are effectively removed from the system. This model places the Apollo 14 HA mare basalts within the confines of a single dynamic process which can explain both major and trace element compositions.

INTRODUCTION

The petrogenesis of basaltic samples returned by the Apollo missions is critical in understanding the composition and development of the Moon's interior and the evolution of the lunar crust. Paramount in the study of mare basalts have been the "pull-apart" efforts on lunar breccias, which have greatly increased the basalt data base. In particular, investigations of basalt clasts, from Apollo 14 breccias have been extremely rewarding. At the Apollo 14 site, the mare basalts form a minor, yet highly significant, component of the lunar crust. For example, the oldest mare basalts have been described from this area (*Taylor et al.*, 1983), as well as the important new VHK (very high potassium) rock-type (*Shervais et al.*, 1984a, 1985).

As a result of such research, three general models have been proposed for basalt petrogenesis: (1) cumulate melting (*Smith et al.*, 1970; *Taylor and Jakes*, 1974); (2) melting of a primitive source (e.g., *Green et al.*, 1971); and (3) assimilation of crustal components by a primitive magma (e.g., *Ringwood and Kesson*, 1976). However, none of these models can, on its own, account for the range in compositions exhibited by high-Al (HA) basalt samples from the Apollo 14 site, which show restricted major element variation, but considerable range in trace element abundances (*Shervais et al.*, 1985).

Earlier work on the Apollo 14 HA mare basalts has described 5 basalt groups (*Dickinson et al.*, 1985; *Shervais et al.*, 1985). The latter authors described a tridymite ferrobasalt/gabbro and an ilmenite ferrobasalt (Group 5) not noted in the work by *Dickinson et al.* (1985). The groupings are based on rare earth and high field strength (HFS) element abundances. These two papers concluded that simple fractional crystallization of a parent magma cannot be responsible for the range displayed in trace element compositions, although the major elements can be generated by such a process (*Dickinson et al.*, 1985). *Shervais et al.* (1985) argued for three distinct source regions below the Apollo 14 site. These authors assumed that the more evolved HA basalts were derived from sources comparatively richer in cpx, containing more trapped liquid, and crystallizing when the magma ocean had greater incompatible element abundances. Both this and a similar approach by *Dickinson et al.* [using a source region proposed for 12038 by *Nyquist et al.* (1981)] cannot generate the observed trace element abundances in all their proposed groups. These authors concluded that variable degrees of cumulate melting of a single source is not responsible for Apollo 14 mare basalt generation.

The process of assimilation has also been addressed. *Shervais et al.* (1985) demonstrated that their 14321-type basalts are generated by assimilation of an "IKFM" KREEP component (intermediate potassium Fra Mauro basalt 15386; *Rhodes and Hubbard*, 1973; *Vaniman and Papike*, 1980) by their 14072-type basalt. *Dickinson et al.* (1985) calculated the effects of assimilation of Apollo 14 KREEP, as well as 15386, by their Group 5 basalts to generate Groups 1-4. They demonstrated that there is better agreement between calculated and observed abundances using 15386 IKFM rather than Apollo 14 KREEP. The Apollo 14 HA mare basalts were generated by 4%-27% assimilation of this composition. However, both *Shervais et al.* (1985) and *Dickinson et al.* (1985) have treated assimilation as a mass balance problem, although the latter authors have

TABLE 1. Numbers, texture, and compositional variation within analyzed mare basalts.

T.S./INAA No.	Texture	Plagioclase			Pyroxene			Olivine
		An	Ab	Or	Fs	Wo	En	Fo
,1115/,1106	O	69-92	7-27	0-4	27-32	6-31	41-67	72
,1118/,1112	G	81-91	9-15	0-1	25-52	6-25	23-68	-
- /,1338	-		-			-		-
- /,1344	-		-			-		-
- /,1345	-		-			-		-
- /,1346	-		-			-		-
,1376/,1318	SO	79-91	9-18	0-2	27-48	7-34	22-63	61-74
,1378/,1329	SO	74-93	7-23	0-3	27-62	7-33	10-66	-
,1382/,1353	O	84-95	5-14	0-2	24-42	9-32	30-62	64-71
,9087/,1347	O	85-94	6-14	0-1	27-34	9-19	42-58	67-70
,9088/,1349	O	87-91	8-12	0-1	28-52	10-26	26-61	-
,9089/,1350	O	77-95	5-20	0-3	25-49	10-28	29-62	62
,9090/,1365	O	80-94	6-18	0-2	27-36	9-33	34-55	65-71
,1471/ -	V	83-94	6-16	0-1		-		68-88
,1473/,1422	V	81-95	4-17	0-2		-		60-71
,1474/,1425	O	80-93	6-19	0-2	25-49	11-36	29-51	58-69
,1475/,1429	O	76-93	7-21	0-3	14-47	8-28	25-61	60-65
,1476/,1432	O	82-94	6-16	0-2	25-51	9-37	23-61	63-68
,1477/,1435	O	78-93	7-18	0-4	24-67	9-36	7-61	60-75
,1478/,1437	O	79-96	4-19	0-3	27-62	9-34	9-64	55-62
,1479/,1439	O	77-94	6-21	0-2	24-51	11-32	22-53	63-72
,1480/,1441	O	85-96	4-14	0-1	25-43	8-34	26-58	56-74
,1481/,1443	O	83-93	7-15	0-2	26-52	9-35	20-63	59-65
,1482/ -	O	75-95	5-23	0-3	25-59	9-34	19-64	58-72
,1483/ -	O	79-93	7-19	0-3	23-55	9-37	8-56	71-86
,1485/ -	O	82-97	3-16	0-3	24-73	11-41	2-61	-
,1486/ -	V	76-95	5-20	0-4		-		71-86

G = granular; SO = sub-ophitic; O = ophitic; V = vitrophyre.

admitted that the magma will also crystallize during assimilation.

Binder (1982, 1985) suggested remelting a layered cumulate in the lunar mantle, followed by storage in the lower crust and 30% fractional crystallization of olivine ± pyroxene as a possible petrogenesis for mare basalts (*Binder,* 1982, Fig. 18, 1985, Fig. 1). This crystallization was coupled with assimilation of residues of urKREEP (*Warren and Wasson,* 1979a) which produced the trace element variability seen in mare basalts.

The present paper refines such models by combining previous Apollo 14 HA mare basalt data with that from 22 new 14321 samples. We demonstrate that "groups" of basalts defined by previous authors are an artifact of sampling and are part of a continuum of compositions generated by a combined assimilation and fractional crystallization (AFC) process between primitive basalt and a KREEP component.

PETROGRAPHY AND MINERAL CHEMISTRY

Freshly sawn surfaces of breccia 14321 were prepared and examined in the facilities at Johnson Space Center. Numerous clasts were extracted for examination. Probe mounts (PM) of 20 mare basalts were prepared and studied using standard petrographic techniques. Mineral chemistry was determined using an automated MAC 400S electron microprobe at the University of Tennessee. Standards, operating procedures, and methods of data reduction have been reported elsewhere (e.g., *Shervais et al.,* 1984b).

Table 1 summarizes the textures and mineral compositions of the basalts studied. These samples are generally ophitic to sub-ophitic basalts dominated by plagioclase and pyroxene, with subordinate olivine phenocrysts. Textures are variable as highlighted in Fig. 1. Sample ,1118 has been granulated (Fig. 1a) and includes two areas of glass (≈ 0.4 mm diameter) containing small (< 0.1 mm) plagioclase phenocrysts. Figure 1b displays the typical texture of the majority of the analyzed basalts. Olivine phenocrysts (see Table 1) can reach > 1 mm diameter and are always rimmed by pigeonitic pyroxene; in ,1118, ,1485, and ,9088 olivine appears to have been totally replaced. In Fig. 1c, ,1476 displays a general ophitic (0.5-0.7 mm), but contains a greater proportion of interstitial glass, whereas ,1474 (Fig. 1d) is much finer grained (0.1-0.3 mm), but still maintains a general ophitic texture.

Euhedral Ti-chromite grains (up to 0.2 mm) are included in olivine, where they are relatively homogeneous (Fig. 2a,b), and also in pigeonite, where TiO_2 typically increases toward the rims. This zonation is considered to be due to continued growth of earlier-formed chromites in the evolving magma, before inclusion in pyroxene, which crystallizes after olivine. In ,1477, reduction of the late-formed Cr-ulvöspinel is evidenced by the association of native Fe and ilmenite with the spinel phase (cf., *El Goresy et al.,* 1972).

Pyroxenes (up to 1 mm) show partial zonation from pigeonite/enstatite cores to augite/ferroaugite rims (Fig. 3). These pyroxenes are interstitial to An-rich plagioclase laths,

generally 0.3-0.7 mm in length, which also display a partial zonation, becoming more Ab- and Or-rich toward the rims (Fig. 5). Plagioclase crystallization in all basalts occurred during pyroxene fractionation, as Al/Ti ratios decrease in more Fe-rich pyroxenes (Figs. 3 and 4). This ratio can be seen to decrease from core to rim of the pyroxene.

Cristobalite is an interstitial (≃ 0.15 mm) phase in some of the basalts studied (e.g., ,1481 and ,9088), where it is associated with opaque glass. Euhedral ilmenites (up to 0.3 mm long), usually found within the opaque glass, are homogeneous (Table 2). However, some variation occurs in MgO from grain to grain within a given sample, reflecting the chemically isolated nature of the residual glass pockets from which ilmenite crystallized.

Three vitrophyres also have been studied (,1471, ,1473, and ,1486); each contains euhedral plagioclase and olivine phenocrysts in an opaque glass. Figure 1e is of vitrophyre ,1471 which contains two populations of olivine phenocrysts. The smaller (0.2 mm diameter), euhedral, and more abundant olivines have a lower Fo content (Fo ≅ 70) than the larger (0.5 mm diameter), subhedral, and less abundant type (Fo ≅ 85). Small (0.25 mm long), rare plagioclase laths are present. Figure 1f is of ,1473 which has more abundant plagioclase laths (up to 0.5 mm long) and large olivine phenocrysts (generally 0.6 mm diameter) containing chromite-ulvöspinel. Glass compositions of the vitrophyres have contrasting compositions: (a) high Al/low Mg (11-31 wt % Al_2O_3; 0.5-7.6 wt % MgO); (b) low Al/high Mg types (2-5 wt % Al_2O_3; 17-23 wt % MgO). Ilmenite and pyroxene are not present in the vitrophyres.

Native Fe is present in all samples, usually < 0.2 mm in diameter, either enclosed in the mineral phases or in the interstices, sometimes too small for analysis. Most show low Ni and Co abundances similar to Apollo 15 mare basalts and

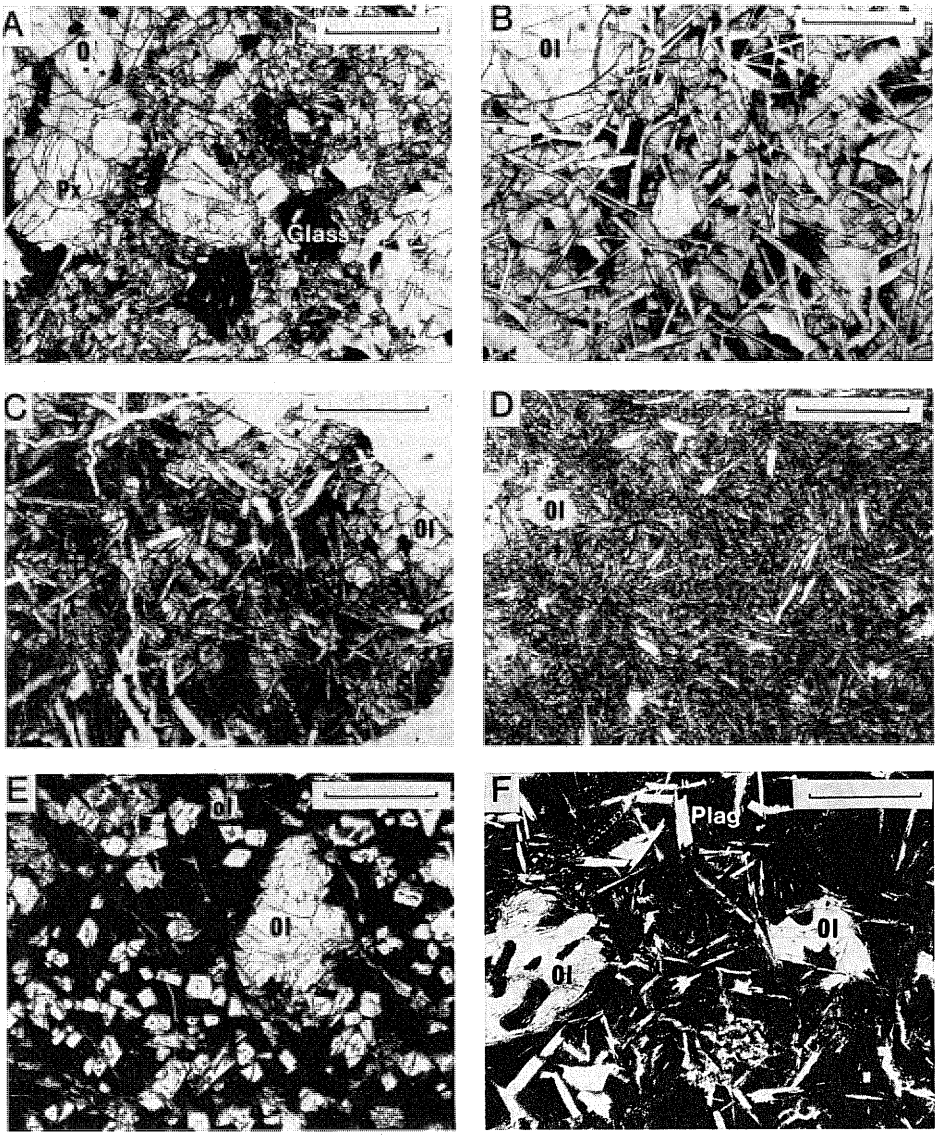

Fig. 1. Photomicrographs depicting the main textural features of the 14321 HA mare basalts. The scale bar represents 1 mm in A-D, and 0.5 mm in E and F. **(a)** Granulated texture of 14321,1118; small areas of glass contain euhedral plagioclase laths. **(b)** General ophitic texture of 14321,1477 which is exhibited by the majority of the 14321 basalts; large olivine phenocrysts (> 1 mm) may be present. **(c)** Sample 14321,1476 also has a general ophitic texture, but contains a much greater proportion of interstitial glass. **(d)** Sample 14321,1474 has a general ophitic texture with olivine phenocrysts, but is much finer grained. **(e)** Olivine vitrophyre 14321,1471 contains two populations of olivine: A large subhedral type (0.5 mm) and a smaller, euhedral type (0.2 mm) set in an opaque glass. **(f)** Olivine vitrophyre 14321,1475 consists of olivine phenocrysts containing chromite, as well as plagioclase laths set in an opaque glass.

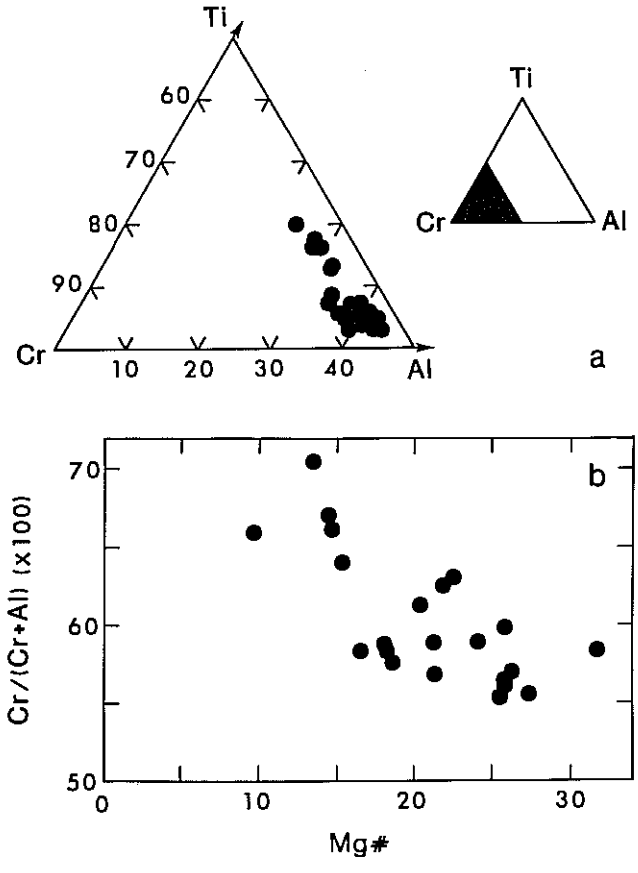

Fig. 2. Graphical representations of chromite-ulvöspinel compositions: (a) the Cr, Al, Ti ternary diagram; (b) Mg# versus 100[Cr/(Cr + Al)].

to previously studied Apollo 14 basalts (*Shervais et al.,* 1983). Basalts which contain native Fe grains with > 1 wt % Ni fall within the field of Apollo 14 mare basalt cumulates (*Shervais et al.,* 1983) or above the field indicating "meteorite contamination." However, four samples (,1115, ,1118, ,1473, and ,1475) have metal compositions which plot above the field of Apollo 14 and Apollo 16 polymict rocks, and meteorite contamination (*Ryder et al.,* 1980).

WHOLE ROCK GEOCHEMISTRY

Analytical Techniques

INAA of 22 new 14321 HA basalt clasts were conducted at Washington University using the procedure of *Lindstrom* (1984). All data were reduced employing the TEABAGS program of *Lindstrom and Korotev* (1982). Uncertainties based on counting rate at the one sigma level are: 1%-2% for Fe, Na, Sc, Cr, Co, La, Sm, and Eu; 3%-5% for Ca, Ce, Tb, Yb, Lu, Hf, Ta, and Th; 5%-15% for Cs, Ba, Nd, and U; 15%-25% for K, Sr, Rb, Ni, and Zr. All samples were analyzed for Ir and Au, which occur below the detection limit of 2-3 ppb, supporting a pristine (i.e., non-impact) origin for these basalts (*Warren and Wasson,* 1979b; *Ryder et al.,* 1980; *Warren et al.,* 1983). Major element compositions were obtained either by INAA (where SiO_2 is calculated by difference) or by broad beam electron microprobe analysis. The latter method involved crushing of INAA samples and fusing on a molybdenum strip in an argon atmosphere followed by quenching. This procedure was carried out at the Johnson Space Center. The elements Ca, Fe, and Na have also been measured by INAA, serving as a check for the fused glass method. In general, there is good agreement, although Fe is sometimes low, possibly due to small Fe-metal grains present in the quench glass.

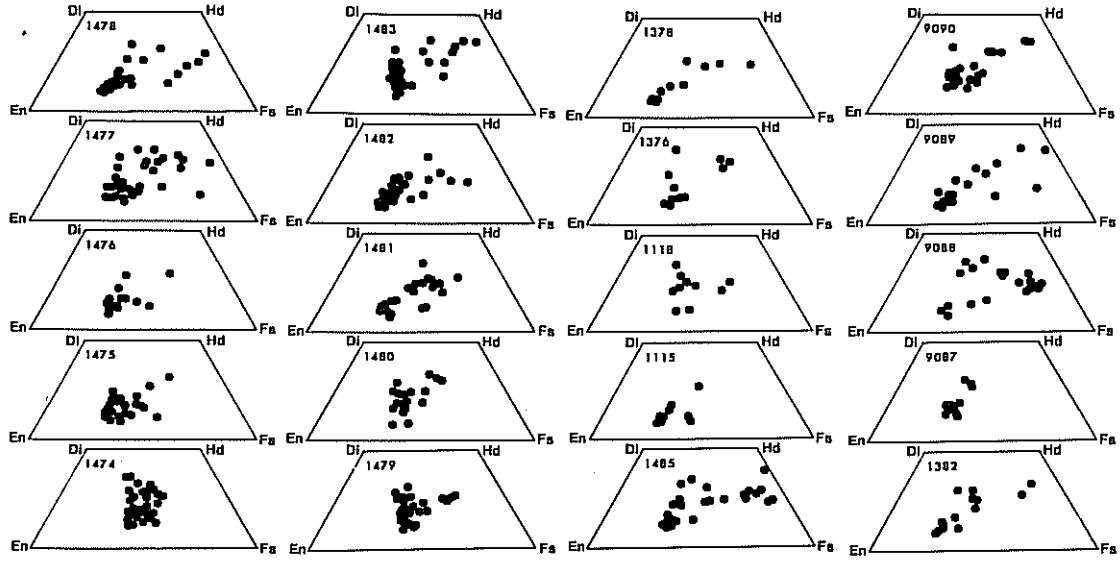

Fig. 3. Pyroxene compositions from all analyzed 14321 HA mare basalts represented on a pyroxene quadrilateral. Note that in practically all cases, there is a general trend toward more Ca- and Fe-rich compositions.

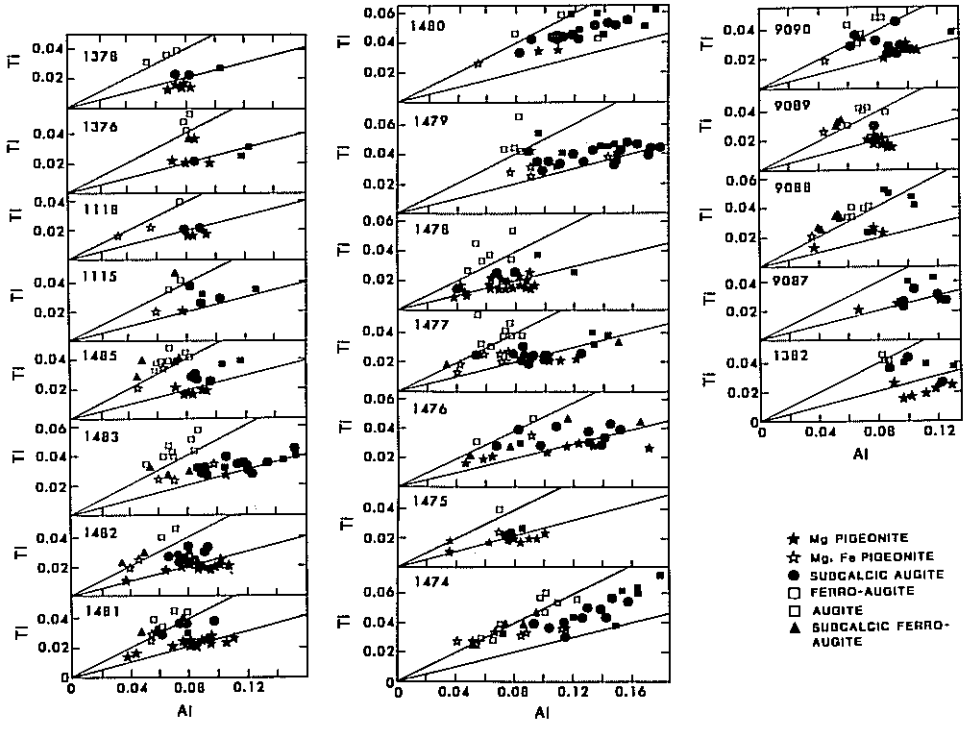

Fig. 4. Pyroxene compositions from all analyzed 14321 HA mare basalts represented on Al versus Ti diagrams. A general decrease in Al/Ti ratio is observed from Ca- and Mg-rich compositions to Fe-rich pyroxenes. This is indicative of plagioclase fractionation during pyroxene crystallization (*Bence and Papike*, 1972).

Results

Whole rock compositions are presented in Table 3. The mare basalts fall within the ranges of low-Ti, high-Al mare basalts reported by *Dickinson et al.* (1985) and *Shervais et al.* (1985), and the Apollo 11 low-K group of *Beaty et al.* (1979). The range of SiO_2 (46.0-50.1) forms a broad negative correlation with MgO (7.00-11.0), indicating these rocks have experienced some degree of olivine and/or pyroxene fractionation. Positive correlations of SiO_2, and negative correlations of Mg#, with the incompatible trace elements (La and Hf) again suggest such a hypothesis.

Large variations are apparent in comparisons of the trace element contents of these basalts. These elements are very sensitive to the many igneous processes that operate during magmatic evolution. The extent to which trace elements are incorporated into different mineral phases varies by several orders of magnitude, according to the respective trace element and the mineral phase considered. These factors all enhance the use of trace elements as petrologic guides of magma evolution, and the trace element behavior is the main subject of the following discussion. For ease of presentation, the trace elements are divided into groups of similar physico-chemical affinity.

Rare earth elements (REE). The REE profiles (Fig. 6) display considerable variation from flat, primitive patterns (at approximately 10 × chondritic abundances) with a small negative Eu anomaly, to evolved LREE-enriched patterns (LREE almost 100 × chondrite abundance), with a large negative Eu anomaly, which mirror KREEP (Fig. 6). Increase in REE abundance (Table 3) is accompanied by an increase in the La/Lu ratio. The new basalt data from this study conveniently fall into three groups on the basis of REE patterns; however, if compared with previous Apollo 14 HA mare basalt REE data (Fig. 6) a continuum of compositions is seen. Therefore, we do not classify the basalts into specific groups but describe them in terms of their La/Lu ratio: Those with a low La/Lu ratio are described as "primitive" and those with a high La/Lu ratio are termed "evolved" types. In addition, the ratio Sm/Eu (a measure of the negative Eu anomaly) increases from the primitive to evolved types.

Compatible elements: Ni, Cr, Sc, and Co. Within the HA basalts analyzed, there is a moderate variation in the

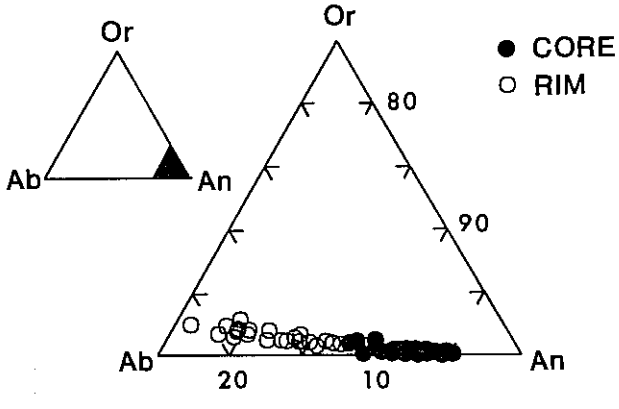

Fig. 5. Core and rim plagioclase compositions represented on an An-Ab-Or ternary diagram, demonstrating an increase in Ab and Or, and decrease in An from core to rim.

TABLE 2. Representative ilmenite analyses from the 14321 basalts.

	,1474	,1475	,1476	,1477	,1478	,1479	,1480	,1481	,1482	,1483	,1485	,1115	,1118	,1376	,1378	,1382	,9087	,9088	,9089	,9090
TiO_2	53.4	53.2	53.4	53.4	54.1	54.4	52.8	52.7	53.1	52.9	53.3	53.0	54.2	53.3	53.2	53.2	54.3	52.8	53.7	52.7
Al_2O_3	0.20	0.25	0.21	0.20	0.12	0.48	0.14	0.23	0.21	0.17	0.21	0.26	0.30	0.39	0.27	0.15	0.59	0.30	0.21	0.23
Cr_2O_3	0.43	0.41	0.39	0.30	0.42	0.31	0.45	0.36	0.21	0.17	0.43	0.41	0.30	0.39	0.27	0.15	0.59	0.30	0.46	0.21
FeO	44.9	44.0	44.5	45.3	44.2	44.3	44.1	45.9	46.4	46.2	44.7	45.0	42.3	46.5	44.5	46.3	42.2	46.8	42.8	46.1
MgO	1.13	1.88	1.42	1.22	1.91	1.04	1.86	0.75	0.63	0.78	1.22	1.19	3.04	0.27	1.17	0.66	2.98	0.59	3.20	0.77
Total	100.06	99.74	99.92	100.42	100.75	100.53	99.35	99.94	100.85	100.22	99.86	99.86	100.14	100.59	99.46	100.62	100.26	100.70	100.37	100.01
Formula on the basis of 3 oxygens																				
Ti	1.000	0.995	0.999	0.998	1.000	1.009	0.993	0.993	0.996	0.995	0.999	0.996	1.000	1.000	1.000	0.996	1.000	0.991	0.991	0.993
Al	0.005	0.007	0.005	0.005	0.002	0.014	0.003	0.006	0.006	0.004	0.006	0.007	0.008	0.003	0.009	0.008	0.005	0.005	0.005	0.006
Cr	0.008	0.008	0.007	0.005	0.008	0.005	0.009	0.006	0.003	0.003	0.008	0.008	0.005	0.007	0.005	0.002	0.011	0.005	0.008	0.003
Fe	0.936	0.914	0.926	0.941	0.908	0.913	0.921	0.961	0.968	0.967	0.934	0.939	0.866	0.970	0.929	0.964	0.864	0.977	0.878	0.966
Mg	0.042	0.069	0.052	0.045	0.070	0.038	0.069	0.028	0.023	0.028	0.044	0.044	0.111	0.009	0.043	0.024	0.108	0.021	0.117	0.028
Total	1.989	1.992	1.990	1.995	1.989	1.978	1.996	1.995	1.997	1.997	1.991	1.994	1.990	1.990	1.986	1.994	1.988	2.000	2.000	1.997
Mg#	4.3	7.0	5.3	4.6	7.2	4.0	7.0	2.8	2.3	2.8	4.5	4.5	11.4	0.9	4.4	2.4	11.1	2.1	11.8	2.8

TABLE 3. Whole rock compositions of 14321 basalts.

INAA #	,1106	,1112	,1318	,1329	,1338	,1344	,1345	,1346	,1347	,1349	,1350	,1353	,1365	,1422	,1425	,1429	,1432	,1435	,1437	,1439	,1441	,1443
PM #	,1115	,1118	,1376	,1378	-	-	-	-	,9087	,9088	,9089	,1382	,9090	,1473	,1474	,1475	,1476	,1477	,1478	,1479	,1480	,1481
Wt (mg)	13.2	11.9	106	72.1	57.3	13.6	21.8	16.1	39.2	36.0	25.6	92.2	83.4	46.0	47.0	46.1	49.4	48.8	32.2	36.9	27.6	52.6
	I	I	P	I	P	P	P	I	P	I	I	I	P	P	P	P	P	P	P	P	P	P
SiO_2	48.7*	49.3*	48.1	47.9*	48.0	48.9	48.3	50.1*	49.4	46.3*	47.1*	48.1*	49.4	46.0	50.2	49.0	48.1	48.9	47.6	48.0	46.7	47.4
TiO_2	1.28	1.91	1.96	2.72	2.06	2.18	2.07	1.66	2.14	2.90	2.22	2.85	2.19	2.72	2.16	2.23	2.65	1.88	2.22	2.07	2.64	2.61
Al_2O_3	11.5	14.5	12.1	12.4	12.0	11.5	12.3	13.1	12.7	13.1	13.4	12.5	12.2	11.3	11.4	11.6	12.1	10.9	13.1	12.6	11.6	11.5
FeO	17.1	14.8	17.0	16.1	16.0	15.9	15.3	14.4	16.0	15.7	15.3	16.5	16.0	17.9	16.7	16.1	16.4	16.9	15.9	15.9	17.2	16.6
MnO	nd	nd	0.20	nd	0.25	0.16	0.16	nd	0.25	nd	nd	nd	0.16	0.23	0.21	0.24	0.33	0.24	0.40	0.22	0.36	0.33
MgO	10.7	7.00	10.2	9.60	9.60	9.49	8.91	9.20	8.05	9.20	8.10	8.40	8.60	11.0	8.80	9.37	8.48	9.28	8.89	8.78	10.7	9.56
CaO	9.90	11.7	10.6	10.4	10.7	10.4	12.0	10.8	11.0	13.3	12.5	10.7	10.5	10.6	10.1	10.6	10.9	10.4	11.3	10.8	10.3	10.5
Na_2O	0.43	0.52	0.50	0.45	0.65	0.53	0.47	0.30	0.58	0.46	0.46	0.55	0.65	0.48	0.48	0.51	0.49	0.51	0.27	0.47	0.41	0.45
K_2O	nd	0.22	0.10	0.16	0.29	0.19	0.20	nd	0.23	nd	nd	nd	0.16	0.03	0.14	0.13	0.05	0.11	0.05	0.14	0.03	0.09
Total	99.61	99.73	100.76	99.73	99.55	99.25	99.71	99.56	100.35	100.96	99.08	99.56	99.86	100.34	100.19	99.78	99.50	99.12	99.73	99.45	99.94	99.04
Sc	57.3	55.0	59.7	56.9	58.2	59.7	61.6	59.8	60.4	60.2	58.7	59.9	59.4	64.1	58.1	61.3	62.0	58.4	58.7	59.3	63.5	58.4
Cr	4190	2906	3819	3230	3188	3386	3264	3284	2870	2734	2980	3144	3470	3770	3070	2975	2920	3150	3315	3220	4000	3485
Co	38.7	40.0	33.4	34.2	34.0	34.6	33.9	33.9	31.8	28.3	32.1	31.2	34.7	32.0	29.9	37.4	28.0	31.9	43.4	33.7	32.6	34.8
Ni	120	80	<100	90	115	150	120	<140	72	60	90	<100	125	<100	<80	<70	<110	49	80	<100	58	<100
Rb	<27	<26	<9	<8	<13	<13	<9	<9	<9	<16	<15	<10	<10	<10	<10	<10	<8	<8	<20	<9	<8	<10
Sr	135	110	72	62	160	150	100	<200	85	100	90	121	100	<100	70	84	60	80	80	55	nd	57
Cs	0.11	0.19	0.18	0.22	0.30	0.26	0.29	0.21	0.26	0.19	0.20	0.20	0.24	<0.20	0.11	0.13	0.15	0.14	0.11	0.15	<0.20	0.18
Ba	150	216	160	170	200	180	200	81	190	155	205	175	170	28	190	190	110	155	83	160	33	130
La	21.1	30.6	20.8	20.3	22.8	21.0	22.7	6.74	24.9	13.2	27.6	20.8	20.5	3.19	23.7	23.3	11.9	21.8	8.35	20.5	3.41	13.5
Ce	59.7	82.9	59.7	56.0	63.8	58.4	63.2	21.0	67.9	37.2	75.2	57.8	57.1	9.3	60.9	62.3	31.2	58.1	22.3	54.1	9.7	35.2
Nd	40	50	30	28	40	35	42	10	40	20	44	33	33	4.3	39	41	18	37	11	30	11	20
Sm	12.1	15.3	10.4	10.5	10.8	10.7	11.6	3.85	11.9	6.76	14.3	10.5	10.5	2.10	12.0	12.1	6.44	11.12	4.75	10.67	2.35	7.59
Eu	1.27	1.67	1.27	1.28	1.33	1.24	1.37	0.672	1.43	1.39	1.53	1.30	1.26	0.62	1.37	1.35	1.03	1.32	0.72	1.30	0.64	1.12
Tb	2.43	3.32	2.40	2.39	2.52	2.49	2.67	1.09	2.71	1.71	3.10	2.40	2.32	0.68	2.63	2.52	1.48	2.46	1.23	2.35	0.75	1.79
Yb	6.72	9.72	7.27	7.20	7.40	6.97	7.61	3.85	8.01	6.33	8.29	7.38	7.27	3.02	7.88	7.93	5.70	7.48	4.49	6.77	2.95	6.33
Lu	1.02	1.33	0.98	0.99	1.00	1.07	1.09	0.57	1.09	0.90	1.24	0.98	0.97	0.44	1.09	1.11	0.82	1.03	0.64	0.98	0.47	0.91
Zr	305	395	280	320	285	390	380	250	400	240	450	330	300	nd	370	400	300	370	230	290	nd	200
Hf	8.14	11.5	8.15	7.94	8.43	8.06	8.58	3.20	9.00	5.75	10.4	8.17	7.95	1.70	8.64	8.62	5.02	8.21	3.62	7.50	1.87	5.43
Ta	0.88	1.31	1.08	1.05	1.11	1.03	1.05	0.42	1.20	0.99	1.22	1.02	0.99	0.45	1.15	1.15	0.89	1.10	0.59	1.06	0.43	0.98
Th	2.07	2.90	1.73	1.84	1.98	2.10	1.95	0.70	2.33	1.59	2.38	1.74	1.79	0.20	2.04	2.40	1.46	1.95	1.35	1.60	0.23	1.50
U	0.32	0.70	0.44	0.42	0.70	0.39	0.57	0.24	0.58	0.50	0.90	0.55	0.42	0.20	0.62	0.58	0.32	0.56	0.23	0.83	0.07	0.48
Ir (ppb)	nd	nd	nd	nd	nd	nd	nd	nd	nd	nd	nd	nd	nd	nd	nd	nd	nd	nd	nd	nd	nd	nd
Au (ppb)	<6	<4	<4	<2	nd	<5	<5	<3	nd	nd	<7	<3	<3	<3	<2	<3	nd	<2	<2	<2	5	<2

* SiO_2 calculated by difference; I = analysis by INA; P = analysis by electron microprobe of fused INAA sample; na = not analyzed; nd = not detected.

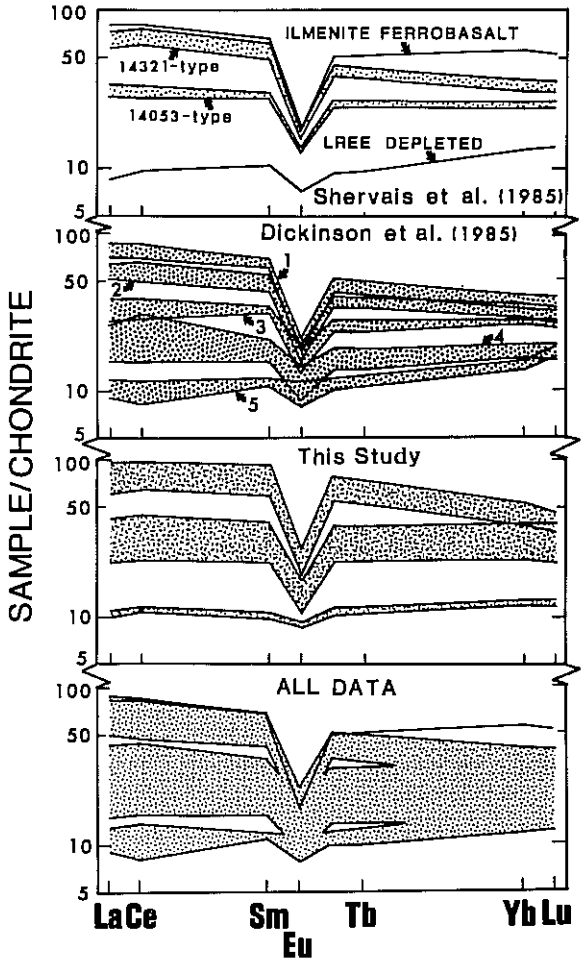

Fig. 6. Rare earth element profiles of all analyzed 14321 HA mare basalts. Each data set (upper 3 diagrams) conveniently falls into groupings, but when all compositions are plotted together, these disappear. Instead, a broad continuum is established (bottom diagram). Although minor gaps still exist, it is evident that 5 basalt groups are not present at the Apollo 14 site. It is expected that these remaining gaps will be filed in as more data is collected.

compatible elements (Ni = 40-180 ppm; Cr = 2734-4190 ppm; Sc = 55.0-64.1 ppm; Co = 28.0-43.4 ppm: Table 3) which classifies these as high-Al basalts corresponding with the major elements described above. Nickel analyses have uncertainties that are too large to be of any constraint and will not be considered further. The variation in Cr and Co cannot be correlated with that in the REE (La/Lu, Sm/Eu), but Sc generally decreases with increasing La/Lu and Sm/Eu.

Large ion lithophile (LIL) elements: K, Rb, Sr, Ba, and Cs. Abundances of K range from 0.03 to 0.25 wt % (Table 3). The high uncertainties associated with Rb and Sr analyses do not allow them to be of any constraint and will not be considered further. Ba displays a considerable range within the 22 analyzed HA basalts (28-216 ppm). K and Ba increase from the primitive basalts to the evolved types, demonstrated by a positive correlation with La/Lu and Sm/Eu. Cs shows moderate variation (0.11-0.30 ppm).

High field strength (HFS) elements: Zr, Hf, Ta, U, and Th. Moderate to large variations in concentration exist within the HFS group. Zr ranges from 200-400 ppm, and an approximate positive correlation between Zr and La/Lu, and Zr and Sm/Eu is noted. However, even better positive correlations are seen with Hf (1.70-11.5 ppm), Ta (0.42-1.31 ppm), U (0.20-0.90 ppm), and Th (0.20-2.90 ppm). These correlations (e.g., Fig. 11e-f) demonstrate concentration of the HFS elements in the basaltic magma from primitive to evolved types.

MODELING

Introduction

It has been previously demonstrated that Apollo 14 HA mare basalt compositions cannot be generated by partial melting of a single source and/or fractional crystallization of a common parent magma (*Dickinson et al.*, 1985; *Shervais et al.*, 1985). A more complicated model for mare basalt petrogenesis by assimilation of urKREEP residues (*Binder*, 1982, 1985) and KREEP (*Dickinson et al.*, 1985; *Shervais et al.*, 1985) has been invoked in order to explain the large variation in trace element contents with limited differences in the major elements. *Binder* (1982, 1985) and *Shervais et al.* (1985) have suggested possible anatexis of KREEPy material in the lower crust by a primitive basaltic magma (e.g., the composition represented by 14321,1422). *Dickinson et al.* (1985) postulated a source for this uncontaminated basaltic magma (Group 5 of their classification) as being an "olivine-orthopyroxene cumulate that crystallized from a magma having chondritic relative abundances." Such a cumulate source would have an inherent

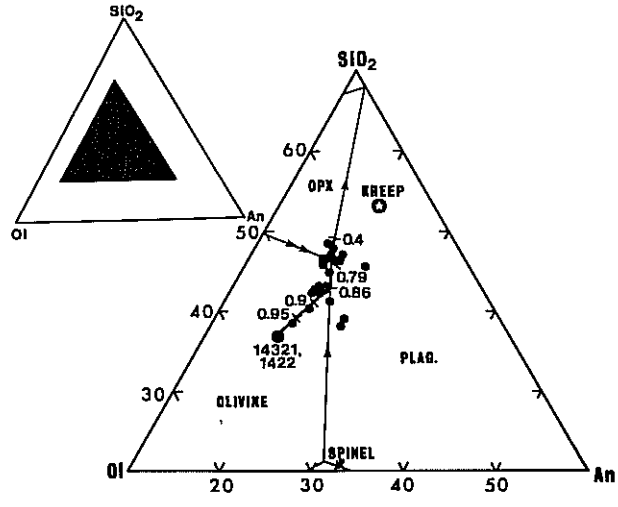

Fig. 7. The major element compositions of the 14321 HA mare basalts from this study represented on a Walker diagram. Phase boundaries are drawn for a Fe/(Fe + Mg) ratio of 0.6, the composition of the evolving parental magma just prior to encountering the plagioclase-olivine cotectic. The fractional amount of melt remaining is shown at various points along the liquidus path. The details of the fractionation modeling are given in the text.

negative Eu anomaly, accounting for the small negative Eu anomaly in the primitive basalts (*Warren*, 1985). *Binder* (1982) suggested a cumulate source consisting of two or more density-graded rhythmic bands whose compositions grade from that of the very low TiO_2 magma source regions (< 0.2% ilmenite) to that of the very high TiO_2 magma source regions (9% ilmenite). However, our research indicates that assimilation alone (i.e., bulk mixing), and even the proposed AFC scheme of *Binder* (1982, 1985), cannot account for all the chemical variations exhibited by the Apollo 14 HA mare basalts (e.g., the Ba and Hf abundances). On the basis of this rationale and the results of our research, we have formulated a combined AFC model for Apollo 14 HA mare basalt petrogenesis.

Modeling Systematics

In the proposed model, KREEP is inferred as an assimilated contaminant by a primitive HA basaltic magma. We have taken the composition of 15386 "IKFM" (*Vaniman and Papike*, 1980) as our KREEP component, so as to be consistent with

TABLE 4. Crystal/liquid partition coefficients used in AFC modeling.

	Pyroxene	Plagioclase	Olivine	Ilmenite	Chromite
La	(0.012)*	0.051	(0.0001)	0.029	0.029
Ce	0.038	0.037	0.0001	0.038	0.038
Sm	0.054	0.022	0.0006	0.053	0.053
Eu	0.100	1.22	0.0004	0.02	0.02
Yb	0.671	0.012	0.02	0.39	0.39
Lu	0.838	0.011	(0.02)	0.47	0.47
Sc	1.6	0.065	0.4	1.5	1.5
Ba	0.013	0.686	0.03	0.005	0.005
Ta	(0.21)	0.04	0.03	0.53	0.53
Hf	0.063	0.05	0.04	1.817	0.38
Th	0.13	0.05	0.03	0.55	0.55

RESULTS

Proportion of Liquid Remaining

	Parent	0.95	0.9	0.86	0.79	0.7	0.6	0.5	0.4	KREEP
SiO_2	46.1	46.8	47.6	48.3	49.1	49.2	49.4	49.6	49.9	50.8
TiO_2	2.73	2.59	2.44	2.31	2.09	2.14	2.21	2.30	2.42	2.23
Al_2O_3	11.3	11.9	12.5	13.1	12.8	12.8	12.8	12.9	12.9	14.8
FeO	17.9	17.4	16.9	16.4	16.5	16.4	16.3	16.1	16.0	10.6
MnO	0.23	0.23	0.22	0.22	0.23	0.24	0.26	0.28	0.30	0.16
MgO	11.1	9.86	8.52	7.34	6.75	6.67	6.58	6.45	6.29	8.17
CaO	10.1	10.7	11.2	11.8	11.9	11.9	11.9	11.8	11.8	9.71
Na_2O	0.48	0.51	0.53	0.56	0.57	0.54	0.52	0.49	0.45	0.73
La	3.19	4.60	6.16	7.54	9.86	13.5	18.1	25.0	31.7	83.5
Ce	9.30	12.9	16.9	20.5	26.4	35.8	47.4	64.6	81.8	211
Sm	2.10	2.77	3.51	4.16	5.26	6.96	9.06	12.2	15.2	37.5
Eu	0.62	0.69	0.77	0.84	0.91	1.04	1.19	1.37	1.60	2.72
Yb	3.84	3.53	4.09	4.59	5.43	6.42	7.59	8.98	10.7	24.4
Lu	0.44	0.51	0.59	0.66	0.78	0.91	1.05	1.32	1.43	3.40
Sc	64.1	65.6	67.2	68.6	71.9	69.3	66.5	63.5	60.2	23.6
Ba	28	42	57	71	91	124	164	214	278	837
Ta	0.45	0.54	0.63	0.71	0.85	1.06	1.31	1.63	2.03	4.60
Hf	1.7	2.25	2.86	3.39	4.29	5.59	7.17	10.3	11.6	31.6
Th	0.2	0.36	0.53	0.68	0.94	1.33	1.82	2.42	3.21	10.0

% crystallized	0-14	15-21	22-60
Olivine	90	40	0
Plagioclase	0	50	30
Orthopyroxene	0	0	60
Ilmenite	0	0	10
Chromite	10	10	0

References: *Binder*, 1982; *Haskin and Korotev* (1977); *Irving and Frey* (1984); *Arth and Hanson* (1975); *McKay et al.* (1986); *Drake and Weill* (1975); *Schnetzler and Philpotts* (1970); *Villemant et al.* (1981).

*Brackets indicate estimated partition coefficient. Chromite REE partition coefficients taken as those for ilmenite.

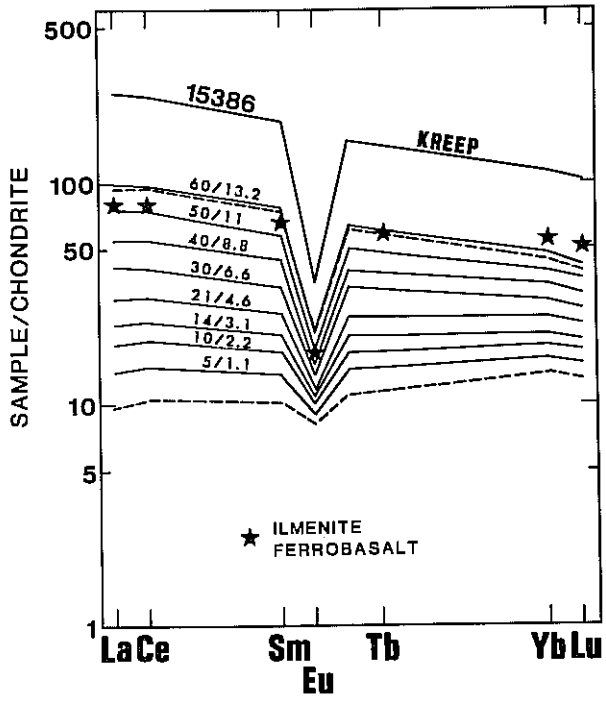

Fig. 8. The range of REE patterns for all Apollo 14 HA mare basalts are modeled using equation (6a) of *DePaolo* (1981) and the phase proportions deduced from major element modeling. Partition coefficients are presented in Table 4. Note that the range of REE patterns can be generated after 60% fractional crystallization of a parental composition represented by 14321,1422. An r value of 0.22 is required, and the numbers on each of the generated patterns represents the percentage crystallized/percentage assimilated. The KREEP composition of *Vaniman and Papike* (1980) was used in these calculations. The ilmenite ferrobasalt of *Shervais et al.* (1985) cannot be effectively generated using this model.

the previous mass balance models of *Dickinson et al.* (1985) and *Shervais et al.* (1985). As the primitive HA magma, the composition of 14321,1422 is taken from our new data as it has the lowest trace element abundances, lowest SiO_2 (46.1 wt %), highest MgO contents (11 wt %), and among the highest Mg# (52.4).

Although the treatment of assimilation as a mass balance problem is a good first approximation, realistically any assimilation will be accompanied by some magma crystallization (*DePaolo,* 1981). The composition of the crystallizing phases will evolve as this process proceeds. We have attempted, where possible, to account for these evolving compositions within our major element modeling, in order to represent a realistic situation. As we envisage a low r value of 0.22 (r = mass assimilated/mass crystallized) for our AFC scheme, the major elements can be effectively modeled by fractional crystallization alone (*DePaolo,* 1981). This may well explain the observation of *Dickinson et al.* (1985) that the major elements may be produced by fractional crystallization alone of a common parent magma. Of course, this conclusion is at variance with the trace element data. The proportions and nature of the fractionating phases can be calculated from phase equilibria (i.e., by representation of data on the Ol-An-SiO_2 pseudoternary). These are applied to the trace elements, upon which assimilation has a profound effect. Such an approach is critical for consistency between major and trace element modeling. This is essential in the development of any model of magma petrogenesis.

Major Element Modeling

A major constraint in any petrologic modeling is the phase equilibria applicable to that particular melt, and numerous experimental investigations of mare basalt liquids have been performed (e.g., *Walker et al.,* 1972; *Kesson,* 1975; *Usselman et al.,* 1975). It was determined that the phase relations could most readily be explained by consideration of the Ol-An-SiO_2 pseudoternary system (often referred to as the "Walker Diagram"), which is extremely useful in representing basaltic compositions. Our new 14321 HA mare basalt data are represented on such a Walker diagram in Fig. 7. The phase boundaries (e.g., cotectics) have been shown to be particularly sensitive to the Fe/(Fe + Mg) ratio of the system (*Walker et al.,* 1973; *Longhi,* 1977). As such, the phase boundaries are drawn for the Fe/(Fe + Mg) of the evolving system just before the evolving melt composition encounters the cotectic (Fe/(Fe + Mg) = 0.6). As stated above, we have modeled the major elements by fractional crystallization only of parent magma 14321,1422, as minor assimilation will have a negligible effect on the major elements (*DePaolo,* 1981).

A least squares regression program was used to calculate the major element compositions of the evolving magma. Olivine and chromite are the first phases to crystallize (*Walker et al.,* 1972). Olivine (90%) and chromite (10%) only fractionate during the first 14% crystallization (Fig. 7). After 14% crystallization, the olivine-plagioclase cotectic is reached and plagioclase (50%), olivine (40%), and chromite (10%) fractionate until 21% of the parental liquid has crystallized. At this point, the olivine-opx-plagioclase peritectic is reached, and olivine fractionation ceases with orthopyroxene becoming the dominant liquidus phase. In our model, we envisage that all olivine has been effectively removed, and no appreciable back reaction occurs at the onset of pyroxene fractionation. Plagioclase (30%), orthopyroxene (60%), and ilmenite (10%) are the fractionating phases until 60% of the parental liquid is solidified. In order to recreate realistic crystallizing conditions, the Fo content of fractionating olivine was calculated iteratively in crystallization increments of 2% using the Mg/Fe ratio of the resultant liquid (method of *Longhi,* 1977). This yielded a range of olivine compositions from 76.9 to 68.0 throughout the period that olivine was on the liquidus. During the first 7% of plagioclase fractionation (up to the peritectic) a composition of An92, Ab8 was used. After the peritectic a plagioclase of composition An79, Ab19 was fractionated. Such compositions were based upon the zonation observed in mare basalt plagioclases. The composition of chromite was estimated from analyzed 14321 HA mare basalts (Mg# = 12.6) as was ilmenite (Mg# = 9.4), and these compositions were kept constant throughout. Pyroxene compositions in a crystallizing magma will evolve from Mg-

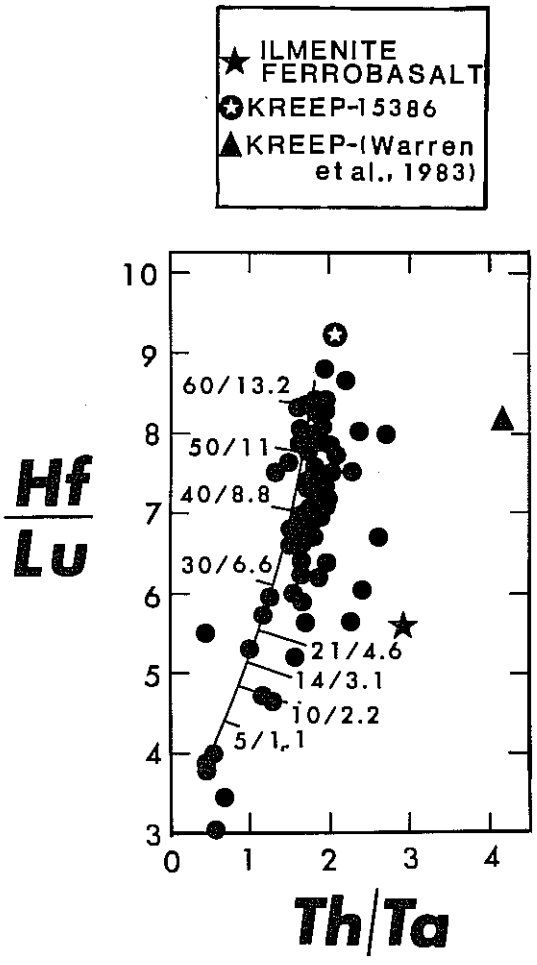

Fig. 9. A plot of Hf/Lu versus Th/Ta which *Shervais et al.* (1985, Fig. 14) used to demonstrate that 15386 was the only feasible contaminant to generate their 14321-type basalts. This plot includes *all* Apollo 14 HA basalt data with an AFC path calculated from 14321,1422 using the phase proportions deduced from the major element modeling. The numbers represent percentage crystallized/percentage assimilated. Note that the ilmenite ferrobasalt cannot be generated by using 15386 as the contaminant. If this basalt has a petrogenesis involving AFC, the KREEP composition of *Warren et al.* (1983) is a more likely composition.

rich/Ca, Fe-poor to Ca and Fe-rich (e.g., *Lindsley and Andersen,* 1983). As a result of such crystallization, an average pyroxene composition of Mg# = 48 is used. This is permissible since olivine fractionation has already depleted the magma in Mg. Results of this modeling are presented in Fig. 7 and Table 4. The calculated crystallization path encompasses all the new Apollo 14 HA mare basalt data presented in this study.

Trace Element Modeling

The trace elements have been modeled by combined assimilation and fractional crystallization, using equation (6a) of *DePaolo* (1981):

$$C_m/C_m^o = F^{-z} + \left(\frac{r}{r-1}\right)\left(\frac{C_a}{zC_m^o}\right)1 - F^{-z}$$

where r = mass assimilated/mass crystallized; z = r + D - 1/r - 1; D = bulk distribution coefficient; C_m^o = concentration of element in parental magma; C_m = concentration of element in residual magma; C_a = concentration of element in assimilated component; F = proportion of liquid remaining.

We have attempted to model critical trace elements from the REE, compatible elements (Sc), LIL (Ba), and HFS (Hf, Th, and Ta) groups. The parental HA basalt composition is again taken as 14321,1422. The proportions of fractionating phases are those calculated from the major element modeling. Crystal/liquid partition coefficients used and results obtained are presented in Table 4. In the following sequence of diagrams, our new basalt data are plotted with other Apollo 14 HA mare basalt data [*Dickinson et al.* (1985); *Shervais et al.* (1985)] from breccia 14321. The Tridymite Ferrobasalt of *Shervais et al.* (1985) is not included in this study as it is a low-Al mare basalt.

In our modeling, the ratio of mass assimilated to mass crystallized (r value) of 0.22 is used. This provides the best fit with our data, using the fractionating phases in the proportions described above. Figure 8 is a chondrite-normalized plot of the range in REE patterns for the Apollo 14 HA basalts and the calculated REE patterns using the model outlined above. Note the important effect pyroxene fractionation has on the HREE, generating the 14321-type basalts of *Shervais et al.* (1985) and Groups 1 and 2 of *Dickinson et al.* (1985). The

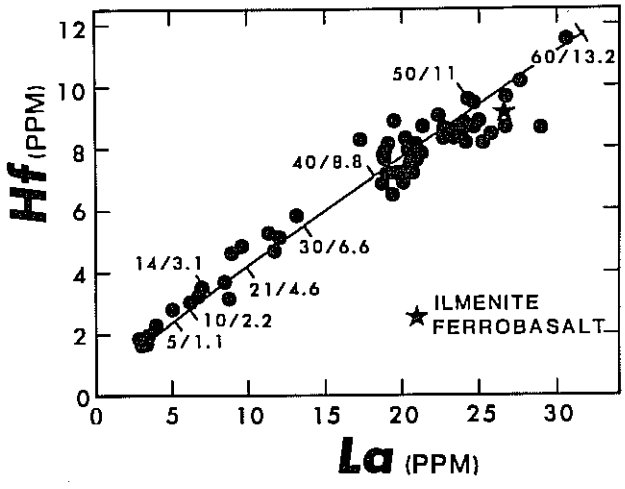

Fig. 10. This plot of La versus Hf is how *Dickinson et al.* (1985) presented their evidence for 5 groups of HA mare basalts at the Apollo 14 site. In this figure all Apollo 14 HA basalt data are plotted, demonstrating that 5 groups do not exist. It may be argued that 2 groups can be defined, but it is evident that as more data are generated, the number of "groups" decreases. As with Fig. 8, we feel that as more basalts are analyzed from the Apollo 14 site, these compositional gaps will disappear. The AFC path has been calculated using the parameters as in previous diagrams. The numbers represent percentage crystallized/percentage assimilated.

highest concentration of REE represents *60% crystallization of parent magma 14321,1422 and 13.2% KREEP assimilation.*

However, the HREE abundances of the highly evolved Ilmenite Ferrobasalt of *Shervais et al.* (1985) cannot be generated using this method. This basalt contains the largest negative Eu anomaly of all the Apollo 14 HA mare basalts which argues for a greater proportion of plagioclase fractionation. The flattening of the REE profile in the HREE could reflect a sympathetic decrease in pyroxene fractionation within the general AFC model.

Figure 9 depicts Hf/Lu versus Th/Ta which is similar to Fig. 14 of *Shervais et al.* (1985), who used this plot to demonstrate that 15386 IKFM was assimilated by a primitive magma to form the 14321-type basalts. We have plotted all Apollo 14 HA basalts on this diagram to demonstrate there are no groups depicted, and an AFC path may be calculated between 14321,1422 and 15386 IKFM (KREEP). The most evolved basalts (i.e., those plotting closest to KREEP) are generated by approximately *60% crystallization of parent magma 14321,1422 and 13.2% KREEP assimilation.* The Group 5 HA

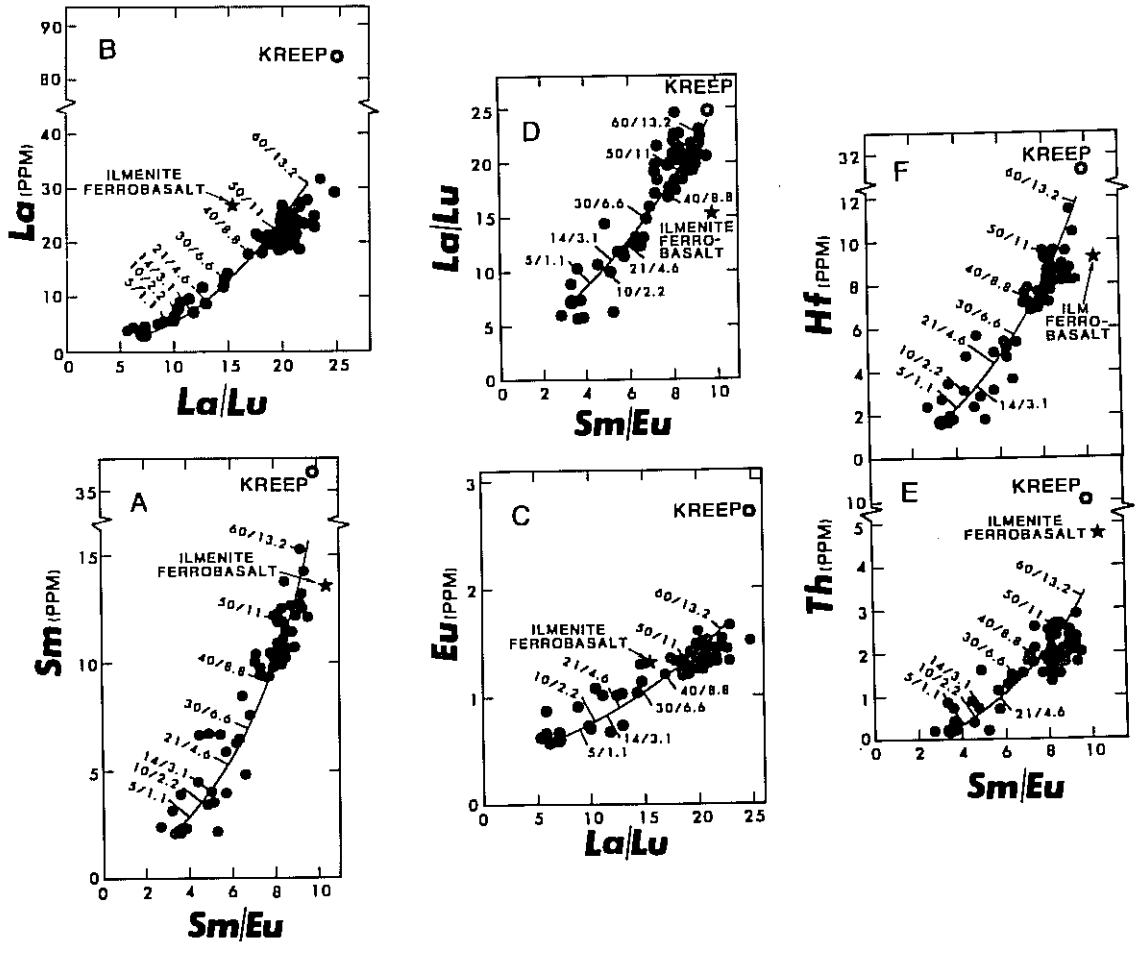

Fig. 11. Six plots involving the rare earth and HFS elements to illustrate that the calculated AFC path is consistent for different elements. In this sequence of diagrams, it is evident that no "groups" of basalts may be defined. It is also evident that each correlation can be consistently represented by our AFC model. The numbers along the AFC path represent percentage crystallized/percentage assimilated. KREEP is shown as an open star symbol. **(a)** Sm versus Sm/Eu is used as a measure of differentiation. Such correlations have been ascribed to short-range unmixing, but with the large range in both Sm and Sm/Eu this process alone is unlikely to be responsible for the Apollo 14 HA mare basalt compositions. These compositions are the result of a more complicated AFC process. **(b)** La versus La/Lu was used by *Shervais et al.* (1985) to demonstrate that their 14321-type basalts could not be generated by fractional crystallization alone. Our figure presents all Apollo 14 HA basalt data and the reasonable fit of an AFC path suggests this process could be responsible for all compositions, not just the "14321-type." **(c)** Eu versus La/Lu which demonstrates the increase of Eu with the steepening of the REE profile (increased La/Lu ratio). **(d)** La/Lu versus Sm/Eu demonstrates that the deepening of the negative Eu anomaly is coupled with the steepening of the REE profile. Such a relationship can be modeled effectively by our AFC scheme. **(e and f)** Th and Hf versus Sm/Eu demonstrate the increase of the HFS elements with the deepening of the negative EU anomaly. Both these relationships may also be effectively represented by our AFC model.

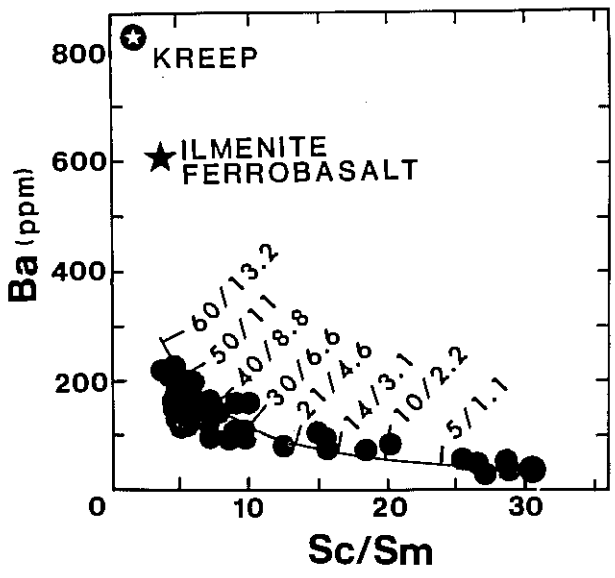

Fig. 12. Ba versus Sc/Sm illustrates the importance of plagioclase fractionation in suppressing Ba enrichment. The correlation between these elements can also be accounted for in our AFC model. The numbers along the AFC path represent percentage crystallized/percentage assimilated. Note that the ilmenite ferrobasalt of *Shervais et al.* (1985) plots between our most evolved basalt and KREEP.

basalts of *Dickinson et al.* (1985) plot below ,1422 on this diagram. These may also be used as parent magmas but would not alter the overall results obtained from our model.

Figure 10 is a plot of La versus Hf abundances, the same as in Fig. 1 of *Dickinson et al.* (1985), who depicted their 5 groups on this basis. All Apollo 15 HA basalt data have been included, and note the general continuum represented. Although one can argue for two groups of basalts (there is a compositional break between La 14-17 ppm and Mg 5.5-7 ppm), five groups cannot be identified. With further data, we expect the compositional gap to be filled and thus argue for a continuum of HA basaltic compositions at the Apollo 14 site. Also, even the Ilmenite Ferrobasalt of *Shervais et al.* (1985) falls on this positive trend, which may argue that the petrogenesis of this rock-type is related to other HA mare basalts. In subsequent diagrams, all previously analyzed Apollo 14 HA basalts are plotted with our new data, to illustrate that 5 groups of basalts do not exist, but are part of a continuum of compositions.

The plot of Sm versus Sm/Eu (Fig. 11a) can be used as an indicator of fractional crystallization. The strong positive correlation would tend to support such a process, but KREEP has both a higher Sm/Eu ratio and Sm abundance which could suggest this correlation represents a mixing path. An AFC path has been calculated between our parent magma and 15386 KREEP. The excellent fit of this path with the data supports our model for HA mare basalt generation at the Apollo 14 site by an AFC process. It is important to note that the Sm/Eu ratio (a measure of the negative Eu anomaly in these basalts) cannot be satisfactorily generated without plagioclase fractionation.

A plot in Fig. 11b of La (ppm) versus La/Lu is similar to Fig. 11 of *Shervais et al.* (1985) who argued that fractionation alone cannot produce this positive correlation. We concur with their conclusion that assimilation of KREEP (represented by 15386 IKFM) by a primitive magma produces their 14321-type basalts. However, we extend this conclusion to include all HA basalt data, except the ilmenite ferrobasalt. This rock-type will be discussed in detail at the end of this discussion. Again the AFC path generated by our model depicts a reasonable fit to the data presented.

The development of the negative Eu anomaly in these basalts is illustrated in Figs. 11c,d, where La/Lu is plotted against Eu and Sm/Eu. These diagrams illustrate that the increase of Eu is primarily controlled by plagioclase fractionation, and the steepening of the REE profile is coupled with the deepening of the negative Eu anomaly. In fact, increases in HFS elements can also be related to the deepening of the negative Eu anomaly (Figs. 11e,f). In all these diagrams, the AFC paths calculated from our model presented above show good agreement with the analyzed HA basalts.

The diagram presented in Fig. 12 is of Ba versus Sc/Sm ratio. This serves to illustrate two points: (1) If the process for basalt evolution is bulk mixing between KREEP and 14321,1422 alone, the Ba abundances would increase too rapidly. Plagioclase fractionation is required to inhibit the Ba increase; (2) Sc is controlled primarily by pyroxene and oxide fractionation, the decreasing Sc/Sm ratio being primarily due to increasing Sm. Our calculated AFC path illustrates the importance of these observations.

DISCUSSION

The above modeling demonstrates how observed HA mare basalt compositions can be generated from a single source (concordant with *Binder,* 1982, 1985). The low r values are in accordance with the previous low estimates of required KREEP contamination (see *Binder,* 1982; *Dickinson et al.,* 1985), and our model requires approximately half the KREEP assimilation of *Dickinson et al.* (1985) (13.2% versus 27%) and considerably lower than the 20% proposed by *Shervais et al.* (1985). The fact that AFC paths (r = 0.22) can be generated for LIL, REE, and HFS elements (Figs. 8-12) strongly indicates assimilation of a KREEP component by a magma fractionating olivine, orthopyroxene, plagioclase, and oxide (calculated from major element modeling) during HA basalt petrogenesis at the Apollo 14 site.

This approach extends the scheme of *Binder* (1982, 1985) by demonstrating the feasibility of crystallizing plagioclase plus oxide, as well as olivine and pyroxene. If only olivine and pyroxene were fractionated, Ba, Eu, and Hf abundances and the Sc/Sm ratio would be much higher than observed, and the larger negative Eu anomaly observed in the more evolved basalts would not be produced. If plagioclase and ilmenite are fractionated, Ba and Hf enrichments are suppressed, while Sc is decreased in the residual liquid after olivine fractionation to produce observed Sc/Sm ratios.

Ilmenite Ferrobasalts

The ilmenite ferrobasalt of *Shervais et al.* (1985) does not show good agreement with our proposed model. However, the petrogenesis of this rock-type can be understood within an AFC model by reference to Figs. 8-12. In Fig. 9, the ilmenite ferrobasalt plots to the right of the main bulk of basalt data. If it had a petrogenesis involving KREEP assimilation, 15386 does not represent this component. Rather, the composition reported by *Warren et al.* (1983) would be a better candidate. In Fig. 11a-f, this rock-type plots either above or below the calculated AFC paths, but its petrogenesis is still consistent with an AFC process with the KREEP composition of *Warren et al.* (1983). However, as noted in Fig. 8, the ilmenite ferrobasalt requires a decrease in the proportion of pyroxene with a subsequent increase in plagioclase fractionation in order to account for the flattening of the HREE and increased Sm/Eu ratio. Figure 10 is the only occurrence of the ilmenite ferrobasalt agreeing with our model. This may be because of similar La/Hf ratios in both 15386 and the KREEP composition of *Warren et al.* (1983). In Fig. 12, the ilmenite ferrobasalt plots above the calculated AFC path. We have argued for increased plagioclase fractionation on account of the REE, but this will restrict Ba in the resulting liquid. Therefore, an increased r value (of approximately 0.5) is required if the ilmenite ferrobasalt is generated by an AFC process. *However, the possibility cannot be ruled out that this rock-type represents a melt from a different source region and is unrelated to the other high-Al mare basalts at the Apollo 14 site.* Our qualitative discussion above is to illustrate the possibility of fitting this rock-type into the general confines of a petrogenesis by an AFC process.

Short-Range Unmixing

A problem encountered in the study of lunar basalts is one of sample size. A study by *Haskin and Korotev* (1977) has demonstrated the effects *short-range unmixing* has on a solidifying lava. This process is similar to fractional crystallization, except there is no large-scale separation of crystallized products from the residual parent liquid (*Lindstrom and Haskin,* 1978). Separations that do occur are far from complete and involve short distances. In effect, short-range unmixing amounts to a sampling problem (*Lindstrom and Haskin,* 1978) because it deals with centimeter-sized inhomogeneities in materials that may be homogeneous on a meter scale. *Lindstrom and Haskin* (1978) noted that correlations between chemical elements among different samples do occur due to short-range unmixing alone. These authors illustrated that in the case of the Apollo 15 basalts, there is a positive correlation between Sm/Eu and Sm (ppm), accountable by short-range unmixing. However, the ranges in Sm/Eu (2.5-4.5) and Sm (3.5-4.5) are much smaller than those in the Apollo 14 HA basalts (2.7-9.3 and 2.1-15.4, respectively). We consider that while short range unmixing may have occurred at the Apollo 14 site, it cannot account for the wide range in trace element abundances observed in these basalts.

CONCLUSIONS

(1) The range of major and trace element compositions in Apollo 14 HA mare basalts can be generated by a combined assimilation and fractional crystallization process involving KREEP. This process produces a continuum of basaltic compositions, rather than strict groupings.

(2) Bulk mixing or assimilation alone between primitive mare basalt and KREEP cannot explain all observed basaltic compositions at the Apollo 14 site.

(3) Major element modeling illustrates that olivine, pyroxene, plagioclase, and oxide are important liquidus phases in the generation of the HA mare basalt suite at the Apollo 14 site.

(4) The proportions of these phases change as the AFC process proceeds. During initial crystallization, only olivine (90%) and chromite (10%) are fractionated. After 15% crystallization of the parental magma, the cotectic is reached and plagioclase (50%) becomes an important liquidus phase with the reduction of olivine (40%), and chromite (10%) remains constant. After 21% crystallization, the peritectic reaction point is reached, and pyroxene (60%) replaces olivine and ilmenite (10%) replaces chromite. Plagioclase is reduced to 30%.

(5) Calculated AFC paths between KREEP (represented by 15386 IKFM) using an r value of 0.22 and the crystallizing phases calculated by major element modeling, show good agreement with observed correlations within the HA mare basalt suite. These indicate that the most evolved HA mare basalts were generated by 60% crystallization of a parental magma (14321,1422) with 13.2% KREEP assimilation.

(6) Short-range unmixing cannot generate the wide range of trace element compositions observed in these basalts.

(7) Ilmenite ferrobasalt cannot be generated within the confines of our model. However, a modified AFC process can account for this composition. The possibility that this rock-type has a petrogenesis unrelated to other Apollo 14 HA basalts cannot be ruled out.

(8) It is envisaged that AFC occurred in the lower lunar crust beneath the Apollo 14 site. Periodic eruptions of mare basalts then occurred that produced the variety of compositions seen in the Apollo 14 breccias.

Acknowledgments. This study would not have been possible without the capable assistance of the Planetary Materials Curatorial Staff at Johnson Space Center, especially Ms. Kim Willis. The sawing of the breccias, the elaborate documentation, and the actual plucking were performed by Kim. We thank Randy Korotev at Washington University for assistance in INA analyses, and Tom See at JSC for help in the fusion process of the basalts. Acknowledgments are due to John W. Shervais, Randy Korotev, and John Jones for constructive reviews of this paper. The research reported in this paper was supported by NASA Grants NGR 9-62 to L. A. Taylor and NAG 9-56 to L. A. Haskin.

REFERENCES

Arth J. G. and Hanson G. N. (1975) Geochemistry and origin of the early Pre-Cambrian crust of northeastern Minnesota. *Geochim. Cosmochim. Acta, 39,* 325-362.

Beaty D. W., Hill S. M. R., Albee A. L., Ma M.-S., and Schmitt R. A. (1979) The petrology and geochemistry of basaltic fragments from the Apollo 11 soil, Part I. *Proc. Lunar Planet. Sci. Conf. 10th,* pp. 41-75.

Bence A. E. and Papike J. J. (1972) Pyroxenes as recorders of lunar basalt petrogenesis: Chemical trends due to crystal-liquid interactions. *Proc. Lunar Sci. Conf. 3rd,* pp. 431-469.

Binder A. B. (1982) The Mare Basalt magma source region and Mare Basalt magma genesis. *Proc. Lunar Planet. Sci. Conf. 13th,* in *J. Geophys. Res., 87,* A37-A53.

Binder A. B. (1985) Mare Basalt genesis: Modeling trace elements and isotopic ratios. *Proc. Lunar Planet. Sci. Conf. 16th,* in *J. Geophys. Res., 90,* D19-D30.

DePaolo D. J. (1981) Trace element and isotopic effects of combined wallrock assimilation and fractional crystallization. *Earth Planet. Sci. Lett., 53,* 189-202.

Dickinson T., Taylor G. J., Keil K., Schmitt R. A., Hughes S. S., and Smith M. R. (1985) Apollo 14 aluminous mare basalts and their possible relationship to KREEP. *Proc. Lunar Planet. Sci. Conf. 15th,* in *J. Geophys. Res., 90,* C365-C374.

Drake M. J. and Weill D. F. (1975) Partition of Sr, Ba, Ca, Y, Eu^{2+} and Eu^{3+}, and other REE between plagioclase feldspar and magmatic liquid: An experimental study. *Geochim. Cosmochim. Acta, 39,* 689-712.

El Goresy A., Taylor L. A., and Ramdohr P. (1972) Fra Mauro crystalline rocks: Mineralogy, geochemistry, and subsolidus reduction of opaque minerals. *Proc. Lunar Sci. Conf. 3rd,* pp. 333-348.

Green D. H., Ware N. G., Hibberson W. O., and Major A. (1971) Experimental petrology of Apollo 12 basalts, I. Sample 12009. *Earth Planet. Sci. Lett., 13,* 85-96.

Haskin L. A. and Korotev R. L. (1977) Test of a model for trace element partition during closed-system solidification of a silicate liquid. *Geochim. Cosmochim. Acta, 41,* 921-939.

Irving A. J. and Frey F. A. (1984) Trace element abundances in megacrysts and their host basalts: Constraints on partition coefficients and megacryst genesis. *Geochim. Cosmochim. Acta, 48,* 1201-1221.

Kesson S. E. (1975) Mare basalts: Melting experiments and petrogenetic interpretations. *Proc. Lunar Sci. Conf. 6th,* pp. 921-944.

Lindsley D. H. and Anderson D. J. (1983) A two pyroxene thermometer. *Proc. Lunar Planet. Sci. Conf. 13th,* in *J. Geophys. Res., 88,* A887-A906.

Lindstrom M. M. (1984) Alkali gabbronorite, ultra-KREEPy melt rock, and the diverse suite of clasts in North Ray Crater feldspathic fragmental breccia 67975. *Proc. Lunar Planet. Sci. Conf. 15th,* in *J. Geophys. Res., 89,* C50-C62.

Lindstrom M. M. and Haskin L. A. (1978) Causes of compositional variations within mare basalt suites. *Proc. Lunar Planet. Sci. Conf. 9th,* pp. 465-486.

Lindstrom D. J. and Korotev R. L. (1982) TEABAGS: Computer programs for instrumental neutron activation analysis. *J. Radioanal. Chem., 70,* 439-458.

Longhi J. (1977) Magma oceanography 2: Chemical evolution and crustal formation. *Proc. Lunar Sci. Conf. 8th,* pp. 601-621.

McKay G. A., Wagstaff J., and Yang S.-R. (1986) Zr, Hf, and REE partition co-efficients for ilmenite and other minerals in high-Ti lunar mare basalts: An experimental study. *Proc. Lunar Planet. Sci. Conf. 16th,* in *J. Geophys. Res., 91,* D229-D237.

Nyquist L. E., Wooden J. L., Shih C.-Y., Weismann H., and Bansal B. M. (1981) Isotopic and REE studies of lunar basalt 12038: Implications for petrogenesis of aluminous basalts. *Earth Planet. Sci. Lett., 55,* 335-355.

Ringwood A. E. and Kesson S. E. (1976) A dynamic model for mare basalt petrogenesis. *Proc. Lunar Sci. Conf. 7th,* pp. 1697-1722.

Rhodes J. M. and Hubbard N. J. (1973) Chemistry, classification, and petrogenesis of Apollo 15 mare basalts. *Proc. Lunar Sci. Conf. 4th,* pp. 1127-1148.

Ryder G., Norman M. D., and Score R. A. (1980) The distinction of pristine from meteorite-contaminated highland rocks using metal compositions. *Proc. Lunar Planet. Sci. Conf. 11th,* pp. 471-480.

Schnetzler C. C. and Philpotts J. A. (1970) Partition coefficients of REE between igneous matrix material and rock-forming mineral phenocrysts - II. *Geochim. Cosmochim. Acta, 34,* 331-340.

Shervais J. W., Taylor L. A., and Laul J. C. (1983) Ancient crustal components in the Fra Mauro breccias. *Proc. Lunar Planet. Sci. Conf. 14th,* in *J. Geophys. Res., 88,* B177-B192.

Shervais J. W., Taylor L. A., and Laul J. C. (1984a) Very high potassium (VHK) basalt: A new type of aluminous mare basalt from Apollo 14 (abstract). In *Lunar and Planetary Science XV,* pp. 768-769. Lunar and Planetary Institute, Houston.

Shervais J. W., Taylor L. A., Laul J. C., and Smith M. R. (1984b) Pristine highland clasts in consortium breccia 14305: Petrology and geochemistry. *Proc. Lunar Planet. Sci. Conf. 15th,* in *J. Geophys. Res., 89,* C25-C40.

Shervais J. W., Taylor L. A., and Lindstrom M. M. (1985) Apollo 14 mare basalts: Petrology and geochemistry of clasts from consortium breccia 14321. *Proc. Lunar Planet. Sci. Conf. 15th,* in *J. Geophys. Res., 90,* C375-C395.

Smith J. V., Anderson A. T., Newton R. C., Olson E. J., Wyllie P. J., Crewe A. V., Isaacson M. S., and Johnson D. (1970) Petrologic history of the moon inferred from petrography, mineralogy, and petrogenesis of Apollo 11 rocks. *Proc. Apollo 11 Lunar Sci. Conf.,* 897-925.

Taylor L. A., Shervais J. W., Hunter R. H., Shih C.-Y., Nyquist L., Bansal B., Wooden J., and Laul J. C. (1983) Pre-4.2 AE mare basalt volcanism in the lunar highlands. *Earth Planet. Sci. Lett., 66,* 33-47.

Taylor S. R. and Jakes P. (1974) The geochemical evolution of the Moon. *Proc. Lunar Sci. Conf. 5th,* pp. 1287-1305.

Usselman T. M., Lofgren G. E., Donaldson C. H., and Williams R. J. (1975) Experimentally reproduced textures and mineral chemistries of high-titanium mare basalts. *Proc. Lunar Sci. Conf. 6th,* pp. 997-1020.

Vaniman D. T. and Papike J. J. (1980) Lunar highland melt rocks: Chemistry, petrology, and silicate mineralogy. *Proc. Conf. Lunar Highlands Crust,* 271-337.

Villemant B., Jaffrezic H., Joron J. L., and Treuil M. (1981) Distribution coefficients of major and trace elements: Fractional crystallization in the alkai basalt series of Chaine des Puys (Massif Central, France). *Geochim. Cosmochim. Acta, 45,* 1997-2016.

Walker D., Longhi J., and Hays J. R. (1972) Experimental petrology and origin of Fra Mauro rocks and soil. *Proc. Lunar Sci. Conf. 3rd,* pp. 797-817.

Walker D., Longhi J., Grove T. L., Stolper E., and Hays J. F. (1973) Experimental petrology and origin of rocks from the Descartes Highlands. *Proc. Lunar Sci. Conf. 4th,* pp. 1013-1032.

Warren P. H. (1985) The magma ocean concept and lunar evolution. *Ann. Rev. Earth Planet. Sci., 13,* 201-240.

Warren P. H. and Warren J. T. (1979a) The origin of KREEP. *Rev. Geophys. Space Phys., 17,* 2051-2083.

Warren P. H. and Wasson J. T. (1979b) Effects of pressure on the crystallization of a "chondritic" magma ocean and implications for the bulk composition of the Moon. *Proc. Lunar Planet. Sci. Conf. 10th,* 2051-2083.

Warren P. H., Taylor G. J., Keil K., Kalleyman G. W., Shirley D. N., and Wasson J. T. (1983) Seventh foray: Whitlockite-rich lithologies, a diopside-bearing troctolitic anorthosite, ferroan anorthosites, and KREEP. *Proc. Lunar Planet. Sci. Conf. 14th,* in *J. Geophys. Res., 88,* B151-B164.